

Deviation of viscous drops at chemical steps

Ciro Semprebon,^{1,*} Silvia Varagnolo,² Daniele Filippi,² Luca Perlini,²
Matteo Pierno,² Martin Brinkmann,³ and Giampaolo Mistura^{2,†}

¹*Department of Mechanical Engineering, University of Edinburgh, Edinburgh EH9 3FB, UK*

²*Dipartimento di Fisica e Astronomia 'G. Galilei' - DFA,
Università di Padova, via Marzolo 8, 35131 Padova, Italy*

³*Experimental Physics, Saarland University, 66123 Saarbrücken, Germany*

We present systematic wetting experiments and numerical simulations of gravity driven liquid drops sliding on a plane substrate decorated with a linear chemical step. Surprisingly, the optimal direction to observe crossing is not the one perpendicular to the step, but a finite angle that depends on the material parameters. We computed the landscapes of the force acting on the drop by means of a contact line mobility model showing that contact angle hysteresis dominates the dynamics at the step and determines whether the drop passes onto the lower substrate. This analysis is very well supported by the experimental dynamic phase diagram in terms of pinning, crossing, sliding and sliding followed by pinning.

PACS numbers: 47.55.D-, 68.08.Bc, 47.55.np, 47.11.-j, 81.65.Cf

Keywords: Drop motion, trapping, contact angle hysteresis, chemical patterns

Contact line motion on solid substrates is crucial in many natural phenomena and technological processes which may have a wide variety of practical applications in daily life, industry and agriculture like rain drops dragged on car windscreens or inkjet printing [1–3]. Macroscopic wetting defects such as chemical patches [4–6], topographic structures [7, 8] and embedded electrodes [9–11] have been proposed to control drop motion. Defects with anisotropic shape or spatial distribution may also induce anisotropic [12, 13] or even unidirectional [14, 15] liquid spreading. Macroscale effects of microscopic defects, instead, are often quantified by means of global descriptors such as the contact angle hysteresis [16]. Predicting the effect of microscopic defects onto drop motion is a challenging task, and the majority of previous studies are restricted to lower dimensions [17–19]. Consequently, to simplify the modelling of drop dynamics in the presence of macroscopic defects [20–22], the intrinsic contact angle hysteresis is often neglected, despite its ubiquity. For example in Refs. [4, 10], the effect of the wetting heterogeneity on the drop dynamics is modelled by a spatial variation of the surface energy. Such models are reasonable only if the contact angle hysteresis interval is narrow compared to the wetting contrast between the substrates.

In this letter, we present experiments and numerical simulations of viscous drops moving on substrates with a large contact angle hysteresis. More specifically, we tracked the deflection of gravity driven drops at a straight wettability step [23], which can be regarded as the limiting case of a pattern of chemical stripes [4, 24]. Our work demonstrates that, in the presence of macroscopic defects, the effects of contact line friction are not negligible and can lead to counter-intuitive results: unexpectedly, the drop crosses more easily when the step is not perpendicular to the sliding direction.

To focus on the interplay between the surface tension

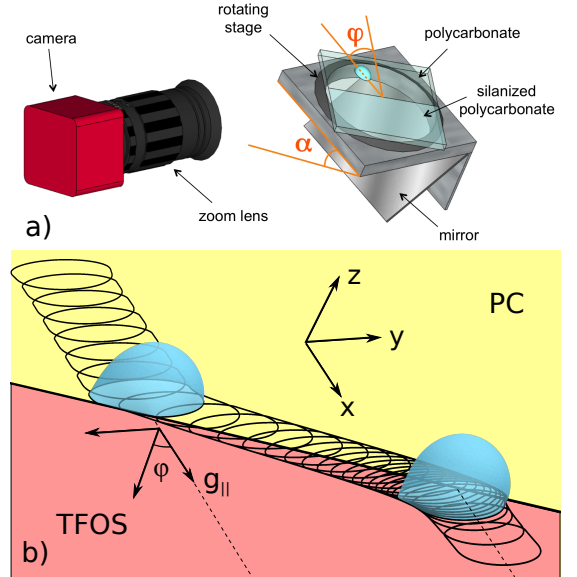


FIG. 1. (color online) a) Sketch of the experimental setup indicating the inclination angle α with the respect to gravity and the tilt angle φ with the respect to the direction of the in-plane body force. b) Rendering of the simulations for $\varphi = 50^\circ$ and $Bo = 1.35$. PC (TFOS) indicates the polycarbonate (silanized) region of the wettability step. The coordinate system x, y, z in the tilted frame employed in the simulations is indicated.

of the free interface and contact angle hysteresis, we used drops of glycerol/water mixture, thus minimising inertial effects [10] and operating in a regime of over-damped interfacial dynamics. As shown in Fig. 1, we tilted the chemical step by an arbitrary angle φ with respect to the direction of the in-plane body force, and mapped out a dynamic phase diagram of the various regimes displayed by the sliding drops. Fundamental insight into the me-

chanics of drop deformation was gained by performing systematic numerical simulations based on a contact line friction model [25]. A typical drop trajectory derived from these calculations is shown in Fig. 1b).

Sliding measurements were performed through the experimental setup depicted in Fig. 1a). We used drops of a 80% w/w glycerol/water solution with density $\rho = 1.21 \text{ g/cm}^3$, viscosity $\eta = 52 \text{ cP}$, i.e. fifty times more viscous than pure water, and with a surface tension $\gamma = 65.3 \text{ mN/m}$ at $T=23^\circ\text{C}$. The substrate was a polycarbonate (PC) slab having a thickness of 5 mm and a side length of 5 cm. To realize the chemical step, half of the original protective cover was kept as a mask for the deposition of a molecular layer of trichloro(1H, 1H, 2H, 2H-perfluorooctyl)silane (TFOS) from the vapor phase. The removal of the cover produced two chemically distinct areas separated by a linear boundary. The wettability of the two regions was characterized by measuring contact angles of drops of the glycerol/water solution. More precisely, the advancing and receding contact angles on the PC region, where the drops were initially deposited, were respectively $\theta_{a,PC} = (88 \pm 2)^\circ$ and $\theta_{r,PC} = (63 \pm 3)^\circ$, while those on the TFOS covered portion, beyond the chemical step, were $\theta_{a,TFOS} = (118 \pm 2)^\circ$ and $\theta_{r,TFOS} = (64 \pm 4)^\circ$.

Drops of volume $V = (40 \pm 2) \mu\text{l}$ were deposited on the already inclined plane by means of a vertically mounted syringe pump. The sample was placed on a manually rotating stage with a central opening that could change the inclination φ of the linear chemical step. The stage was mounted on a rotating tilting support whose inclination angle α could be set by a computer with 0.1° accuracy [5]. The drop was lightened by two white LED backlights. The lateral profile of the drop was viewed with a CMOS camera mounted along the rotation axis of the plate and equipped with a macro zoom lens. By moving the camera, it was possible to focus on the image of the drop contact line reflected by a mirror mounted under the sample holder at 45° with respect to the substrate. Acquired images, where drops appear dark on a light background, were analysed through a custom-made LabVIEW script [26].

Varying α between 25° and 60° , the in plane component of the body force can be described by a Bond number $\text{Bo} = \rho g V^{2/3} \sin \alpha / \gamma$ (where g is the gravity acceleration) comprised between 0.9 and 1.8, as shown in Fig. 2b). The typical velocities of the drop steadily sliding on the PC region before touching the step ranged between $U \sim 0.1 \text{ mm/s}$ and $U \sim 10 \text{ mm/s}$, cf. also Fig. 2. Accordingly, the maximum Weber and Capillary number of the drop with dimension $L_0 \sim V^{1/3}$ were $\text{We} = \rho U^2 L_0 / \gamma \sim 3 \cdot 10^{-3}$ and $\text{Ca} = \eta U / \gamma \sim 0.01$, respectively. Capillary waves on the drop interface that may be excited during collision with the chemical step are quickly damped away as the Ohnesorge number $\text{Oh} = \text{Ca} / \text{We}^{1/2} \sim 0.15$ is close to unity. In addition, when crossing the chemical step the contact line velocity is further reduced to the order of

$U \sim 0.01 \text{ mm/s}$: a regime where the contact line mobilities on many substrates are more favourably described by the Molecular Kinetic model [27] rather than by viscous dissipation in the fluid wedge [28]. Hence, we treated the drop shapes in our simulations as quasi-static and governed by an interplay of interfacial tension, gravity, and contact line friction.

The assumption of a dissipation localized at the moving contact line is not valid for interfaces in contact to substrates with low contact angle hysteresis. In these particular cases, viscous dissipation in the contact line region, and to a smaller extent also in the bulk, dominate drop motion [29], and solutions of the full-scale fluid dynamic problem are required [4]. The essential physics of the present experimental system, instead, can be reproduced with a minimal model based on contact line friction that naturally combines static and dynamic contact angle hysteresis [25, 30].

In the contact line friction model, the shape of the liquid interface is assumed to be in mechanical equilibrium, and therefore at each instant fulfils the Laplace law

$$\Delta P + \rho g_{\parallel} x = \gamma \kappa \quad (1)$$

where ΔP is the pressure jump across the liquid interface at $x = 0$, γ the liquid-vapour tension, κ the local mean curvature, and $g_{\parallel} = g \sin \alpha$ the in-plane component of the acceleration of gravity acting in the downhill x -direction, cf. also Fig. 1. For simplicity, we neglected the component $g_{\perp} = g \cos \alpha$ normal to the substrate in our calculations. For a given contour Γ of the contact line, being not necessarily in mechanical equilibrium, the shape Σ of the free liquid interface is described by a minimum of the energy functional

$$\mathcal{E}\{\Sigma\} = \gamma A_{lv} - \rho g_{\parallel} V \langle x \rangle \quad (2)$$

where A_{lv} is the area of the free interface, while $\langle x \rangle$ denotes the x -coordinate of the drops' center of mass. The surface Σ is subject to the global constraint of a fixed liquid volume V . We employed the free software Surface Evolver [31] to represent the free interface with a triangulated mesh and minimize the energy Eq. (2) with standard minimization algorithms. The motion of the contact line was obtained by displacing the elements in contact with the substrate into the local normal direction, according to the algorithm described in Ref. [25].

As we were operating exclusively in the limit of small contact line velocities in Fig. 2a), we employed a linear relation between contact line velocity and dynamic contact angles

$$u = \begin{cases} u_a(\theta - \theta_a) & \text{for } \theta \geq \theta_a \\ u_r(\theta - \theta_r) & \text{for } \theta \leq \theta_r \end{cases}, \quad (3)$$

where u_a and u_r were assumed to be constant over a homogeneous portion of substrate. To match simulations

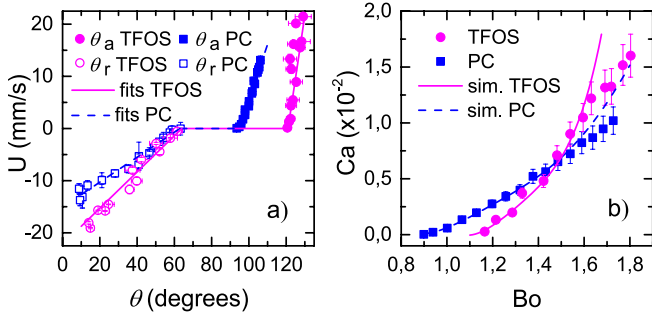


FIG. 2. (color online) a) Experimental measurements of the dynamic advancing and receding angles for PC and TFOS substrates, with linear fits providing the phenomenological parameters for the simulation. Positive (negative) velocities refer to advancing (receding) motion. b) Relation between Bo and Ca for drops in steady motion on PC and TFOS. Lines are the numerical results.

with the experiments, the phenomenological parameters u_a and u_r were obtained by fitting the relation between contact line velocity and dynamic contact angles derived from the experiments on PC and TFOS substrates in Fig. 2a): $u_{a,PC} = 61.6 \text{ mm s}^{-1}\text{rad}^{-1}$, $u_{r,PC} = 13.7 \text{ mm s}^{-1}\text{rad}^{-1}$, $u_{a,TFOS} = 138 \text{ mm s}^{-1}\text{rad}^{-1}$, $u_{r,TFOS} = 19.9 \text{ mm s}^{-1}\text{rad}^{-1}$. In Fig. 2b) we report a direct comparison of the relation between dimensionless drop speed Ca and driving force Bo with the experimental data of steady drops sliding on homogeneous PC and TFOS. Very good agreement was found on both substrates for $Bo < 1.6$ while numerical data overestimate the experimental results at larger Bond numbers. A possible cause for the discrepancy at high Bond numbers is the transition to a regime where the viscous dissipation in the bulk cannot be any more neglected.

We observed four distinct scenarios for the drop approaching the chemical step as summarized in Fig. 3: a) at low Bo and φ the drop is simply pinned at the step; b) at high Bo and intermediate φ the drop crosses the step; c) at high φ the drop glides along the step without crossing it; d) at intermediate Bo and φ the drop glides for a short distance (at least 2 mm) along the step until arrest, and remains pinned. By systematically varying the angles α and φ , we constructed the dynamical phase diagram plotted in the graph of Fig. 3e). Filled symbols of different colors and shapes represent the path followed by the drop approaching the chemical step. No data are reported for $Bo \leq 1$ because drops slide very slowly and it was very difficult to distinguish the different crossing cases. The regions identifying the four regimes are delimited by connected open symbols obtained from the analysis of systematic numerical simulations. They show a good agreement with the experimental results, considering the unavoidable presence of various sources of defects and noise in the system. In particular, the transition curve separating the pinning region from the gliding and

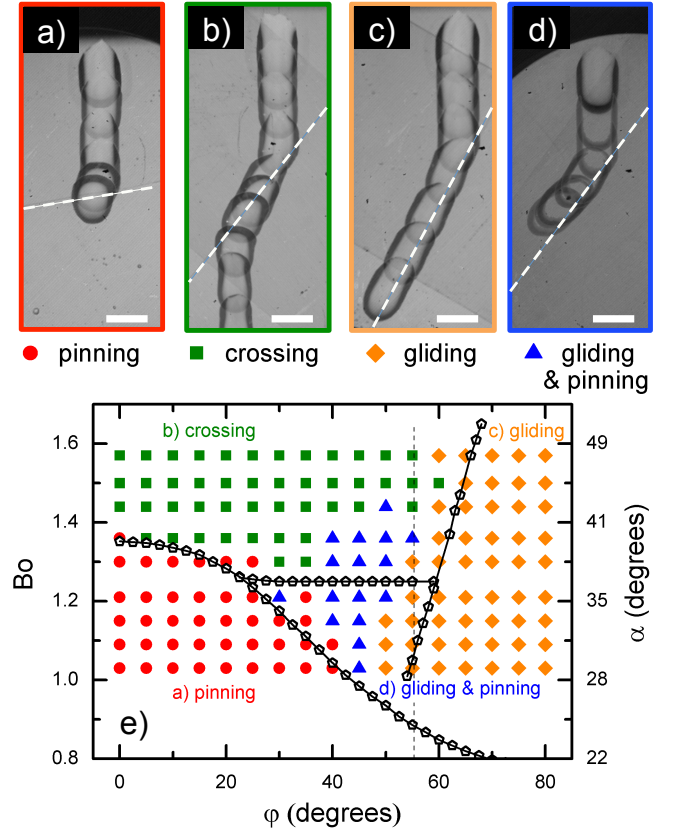


FIG. 3. (color online) Sequence of the four possible drop trajectories exhibited by a drop approaching the chemical step: a) the drop pins; b) the drop crosses the step; c) the drop slides along the step; d) the drop partially slides along the step and pins in a later stage. The dashed inclined lines mark the chemical step and the horizontal scale bars correspond to 5 mm. e) Dynamical phase diagram showing the four regions in the φ - Bo space. Filled symbols refer to experiments, while open symbols are evinced from simulations. Connecting lines are guide for the eye. See text for further details.

pinning one occurs at somewhat smaller φ values. This could be due to the presence of substrate defects that enhance the pinning of the drop. Furthermore, the transition with the gliding region occurs at larger φ values, suggesting that most of defect are located on the TFOS side.

The results present two counter-intuitive aspects. First, one would expect the minimum Bond number Bo_{min} necessary to let the drop cross the step to grow with φ , because the component of the body force perpendicular to the step decreases as $\cos \varphi$. Instead we observed a decrease of Bo_{min} as φ increased. In other words, the optimal direction for crossing is not perpendicular to the step. To prove that such unexpected result is determined by the intrinsic hysteresis, we performed simulations in the absence of static contact angle hysteresis by taking two different equilibrium angles at the two sides of the step, with the drop crossing from

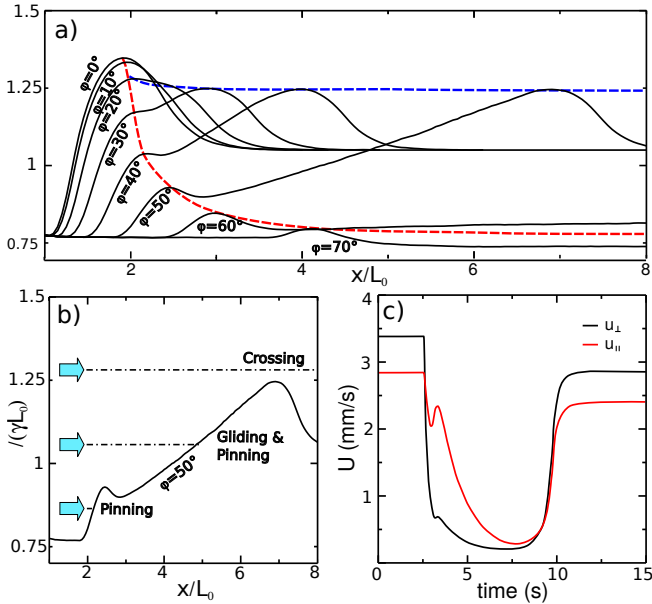


FIG. 4. (color online) a) Force landscape of the crossing mechanism for various values of φ . The dashed lines indicate the trend of the two peaks present in the curves. b) Construction of three crossing scenarios for the case $\varphi = 50^\circ$. c) Parallel and perpendicular velocity components of the drop centre of mass when crossing the step for $\varphi = 50^\circ$ and $Bo = 1.35$. Series of force curves as a function of the position x of the center of mass, normalized by $L_0 = V^{1/3}$, for φ varied in steps of 10° . Here the drop is initially placed at $x = 0$, while the position of the chemical step shifted forward with increasing φ for better visibility.

the more hydrophilic to the more hydrophobic. Regardless of the chosen combination of angles, we always observed a monotonous increase of body force proportional to $1/\cos \varphi$, as suggested by a simple decomposition of the body force along the component perpendicular and parallel to the straight boundary. In this case the dynamical phase diagram is simplified, showing only the crossing and gliding regimes. The second counter-intuitive aspect is the re-entrant shape of the diagram in the range $50^\circ \lesssim \varphi \lesssim 60^\circ$: for φ around 55° (see dashed line in Fig. 3e)), rising Bo from low to high values we first found the transition between pinning and gliding. Upon increasing Bo we noticed a transition between gliding and gliding followed by pinning. Only at higher values of Bo we observed drops crossing the step. This means that the increase of the body force can induce pinning of a drop otherwise in motion.

To gain insight into the mechanism that hinders or allows crossing of the drop, we computed an associated force landscape. To this end we dropped the potential energy term in Eq. (2) and applied instead an additional global constraint on the downhill center of mass position, $\langle x \rangle$. The y -component of the center of mass was instead allowed to freely adapt to the value that minimizes the

total energy. To compute the force landscape we quasi-statically shifted the position of the center of mass along the direction of the body force. In this case the retaining force in our simulations is given by the Lagrange multiplier μ related to the constraint of a fixed $\langle x \rangle$. At each increment we allowed the contact line to relax until all the contact angles lied within the static hysteresis interval. As shown in the series of force curves in Fig. 4a), when the drop collides with the step, μ rises because of the contact line deformation. For small φ the curves exhibit a single peak, which determines the minimum body force required to cross the step. At larger φ the curves show a second peak. Here the new rise of the force is clearly related to the shift of the drop from the low hysteresis PC to the high hysteresis TFOS region. Similarly to what observed for the case of depinning from an initially circular contact line [25], the second peak occurs when the drop escapes from the self-created constriction of the contact line. With increasing φ the magnitude of both peaks decreases. While the first peak vanishes in the limit $\varphi \rightarrow 90^\circ$, the second peak approaches a constant value. Furthermore the distance of the second peak from the contact point asymptotically diverges when φ increases, and completely disappears from our simulation domain for $\varphi > 50^\circ$.

The analysis of the landscape allows to identify all four experimentally observed dynamical regimes for a drop approaching the tilted chemical step. In Fig. 4b) the body force is represented by blue arrows on the left side. If Bo is lower than the first peak, the drop simply pins after touching the step. If the value of Bo falls into the interval between the two peaks, the drop glides along the step and pins afterwards. Only if Bo exceeds the height of the second peak, the drop crosses the step. The sequences of peaks as a function of φ accurately match the transition lines in Fig. 3 between crossing and pinning, and between crossing and gliding with pinning. The absence of the second peak at larger φ implies that the drop is entirely repelled by the step, corresponding to the gliding observed in the experiments. The boundary of the gliding region cannot be determined from the analysis of the force landscape. The line displayed in Fig. 3 is obtained by mapping the results of several sequences of simulations, and can be approximately described by $Bo \simeq Bo_\perp / \cos \varphi$. Here $Bo_\perp \simeq L(\cos \theta_r - \cos \theta_a)$, L being the projection of the drop elongation perpendicular to the step. Such relation implies that the body force can be split in two independent components. While without contact angle hysteresis this is valid for the full range of φ , with hysteresis the decomposition is valid only for large φ , and in both cases it corresponds to the transition to gliding. Figure 4c), reports the two components of the velocity profile corresponding to the trajectory shown in Fig. 1b). For drops coming from the upper (PC) substrate, the first touch of the chemical step causes a fast decrease of the drop velocity. After a local minimum, the

velocity slightly increases in the parallel component, due to squeezing and alignment of the drop along the step. Consequently the drop starts a slow side-ward shift to the lower (TFOS) substrate, which causes a further decrease of the velocity. Eventually the drop escapes from the chemical step and the retaining force decreases, causing a quick acceleration, until reaching a steady motion on the TFOS substrate.

In summary, we have studied with experiments and numerical simulations viscous drops crossing a tilted chemical step to address the effect of intrinsic contact angle hysteresis and found a rich drop dynamics, displaying four different regimes. We demonstrated that the body force required to cross the step increases as $\sim 1/\cos\varphi$ in the absence of intrinsic hysteresis or for sufficiently large inclinations φ . Only without static contact angle hysteresis, the retaining force can be split in two orthogonal components, otherwise the coupling induced by the hysteresis gives rise to the complexity of the observed scenario. In this work we have considered drops crossing from a region of lower to a region of higher advancing contact angles, being the receding angle approximately the same. Correspondingly, the transition is from lower to higher contact angle hysteresis. The opposite scenario, involving a variation only in the receding angles, would not present the same counter-intuitive aspects, because the rise of the second peak in the force landscape is strictly due to the drop deformation of the front edge. Our results show that intrinsic hysteresis can be exploited to control drop motion in open microfluidic devices, particularly if they rely on breaking of the reflection symmetry.

C.S. thankfully acknowledges Halim Kusumaatmaja and Timm Krüger for inspiring discussions. M.B. and G.M. gratefully acknowledge the Vigoni exchange program between the Ateneo Italo-Tedesco and the German Academic Exchange Service (DAAD). We are particularly grateful to Paolo Sartori for kind support in the set-up preparation.

* ciro.semprebon@ed.ac.uk

† giampaolo.mistura@unipd.it

- [1] D. Bonn, J. Eggers, J. Indekeu, and J. Meunier, *Rev. Mod. Phys.* **81**, 739 (2009).
- [2] D. Quéré, *Annu. Rev. Mater. Res.* **38**, 71 (2008).
- [3] K. Liu, X. Yao, and L. Jiang, *Chem. Soc. Rev.* **39**, 3240 (2010).
- [4] S. Varagnolo, D. Ferraro, P. Fantinel, M. Pierno, G. Mistura, G. Amati, L. Biferale, and M. Sbragaglia, *Phys. Rev. Lett.* **111**, 066101 (2013).
- [5] S. Varagnolo, V. Schiocchet, D. Ferraro, M. Pierno, G. Mistura, M. Sbragaglia, A. Gupta, and G. Amati, *Langmuir* **30**, 2401 (2014).
- [6] A. Nakajima, Y. Nakagawa, T. Furuta, M. Sakai, T. Isobe, and S. Matsushita, *Langmuir* **29**, 9269 (2013).
- [7] Y. V. Kalinin, V. Berejnov, and R. E. Thorne, *Langmuir* **25**, 5391 (2009).
- [8] J. C. Baret, M. M. J. Decré, S. Herminghaus, and R. Seemann, *Langmuir* **23**, 5200 (2007).
- [9] D. J. C. M. 't Mannetje, C. U. Murade, D. van den Ende, and F. Mugele, *Appl. Phys. Lett.* **98**, 014102 (2011).
- [10] D. J. C. M. 't Mannetje, S. Ghosh, R. Lagraauw, S. Otten, A. Pit, C. Berendsen, J. Zeegers, D. van den Ende, and F. Mugele, *Nat. Commun.* **5**, 3559 (2014).
- [11] P. Brunet, M. Baudoin, O. B. Matar, and F. Zoueshtigh, *Physical review. E, Statistical, nonlinear, and soft matter physics* **81**, 036315 (2010).
- [12] O. Bliznyuk, H. P. Jansen, E. S. Kooij, and B. Poelsema, *Langmuir* **26**, 6328 (2010).
- [13] L. Courbin, E. Denieul, E. Dressaire, M. Roper, A. Ajdari, and H. A. Stone, *Nat. Mater.* **6**, 661 (2007).
- [14] K.-H. Chu, R. Xiao, and E. N. Wang, *Nat. Mater.* **9**, 413 (2010).
- [15] N. A. Malvadkar, M. J. Hancock, K. Sekeroglu, W. J. Dressick, and M. C. Demirel, *Nat. Mater.* **9**, 1023 (2010).
- [16] C. Semperebon, S. Herminghaus, and M. Brinkmann, *Soft Matter* **8**, 6301 (2012).
- [17] J. F. Joanny and M. O. Robbins, *J. Chem. Phys.* **92**, 3206 (1990).
- [18] N. Savva and S. Kalliadasis, *J. Fluid Mech.* **725**, 462 (2013).
- [19] D. Herde, U. Thiele, S. Herminghaus, and M. Brinkmann, *Europhys. Lett.* **100**, 16002 (2012).
- [20] H. Kusumaatmaja and J. M. Yeomans, *Langmuir* **23**, 956 (2007).
- [21] M. Sbragaglia, L. Biferale, G. Amati, S. Varagnolo, D. Ferraro, G. Mistura, and M. Pierno, *Phys. Rev. E* **89**, 1 (2014).
- [22] A. Cavalli, M. Musterd, and F. Mugele, *Phys. Rev. E* **91**, 1 (2015).
- [23] M. A. Nilsson and J. P. Rothstein, *Phys. Fluids* **24**, 062001 (2012).
- [24] S. Suzuki, A. Nakajima, K. Tanaka, M. Sakai, A. Hashimoto, N. Yoshida, Y. Kameshima, and K. Okada, *Appl. Surf. Science* **254**, 1797 (2008).
- [25] C. Semperebon and M. Brinkmann, *Soft Matter* **10**, 3325 (2014).
- [26] T. Toth, D. Ferraro, E. Chiarello, M. Pierno, G. Mistura, G. Bissacco, and C. Semperebon, *Langmuir* **27**, 4742 (2011).
- [27] T. D. Blake, a. Clarke, J. DeConinck, and M. J. DeRuijter, *Langmuir* **13**, 2164 (1997).
- [28] R. Fetzer and J. Ralston, *J. Phys. Chem. C* **114**, 12675 (2010).
- [29] N. Le Grand, A. Daerr, and L. Limat, *J. Fluid Mech.* **541**, 293 (2005).
- [30] M. Musterd, V. van Steijn, C. R. Kleijn, and M. T. Kreutzer, *Phys. Rev. Lett.* **113**, 066104 (2014).
- [31] K. A. Brakke, *Philos. T. Roy. Soc. A* **354**, 2143 (1996).